Analyst

COMMUNICATION

View Article Online
View Journal | View Issue

Cite this: *Analyst*, 2021, **146**, 1835

Received 17th December 2020,
Accepted 14th January 2021

DOI: 10.1039/d0an02408b

rsc.li/analyst

A ratiometric electrochemiluminescent cytosensor based on polyaniline hydrogel electrodes in spatially separated electrochemiluminescent systems†

Gen Liu, [a,b,c] Zixuan Chen, [a] Bao-Kang Jin[c] and Li-Ping Jiang *[a]

Here, we proposed a ratiometric electrochemiluminescent (ECL) strategy in spatially multiplied ECL systems. By the specific recognition of hyaluronic acid with proteoglycan CD44 and epidermal growth factor with epidermal growth factor receptor on the cell surface, the cells were labelled with potential-resolved ECL probes, namely $Ru(bpy)_3^{2+}$ and g-C_3N_4, respectively. The as-proposed cytosensor provides a multichannel ECL protocol to improve the throughput, which may push the application of ECL for the cellular immunoanalysis.

Electrochemiluminescence (ECL) integrates the advantages of electrochemistry and chemiluminescence. Due to its weak background interference, simplified optical setup, and good temporal-spatial control, ECL has been a powerful analytical tool in the fields of pharmaceutical analysis, immunoassay, environmental analysis, and clinical diagnosis.[1–4] Particularly, ECL measurements for cancer cells have been extensively studied.[5–8] The detection is usually based on a type of cell–surface marker, which results in single emission intensity changes. However, there is still room for improvement. On the one hand, most of the cancer cells have more than one marker, and thus, the detection *via* multiple over-expressed markers on the cell surface will increase the reliability of cancer diagnosis. On the other hand, the absolute values of an ECL signal may introduce false positive or negative errors due to instrumental inefficiency or some environmental changes.[9–11] Therefore, the development of a ratiometric ECL cytosensor based on multiple markers on the cell surface is very necessary for the prediction of cancer.

[a]*State Key Laboratory of Analytical Chemistry for Life Science, School of Chemistry and Chemical Engineering, Nanjing University, Nanjing, 210023, China. E-mail: jianglp@nju.edu.cn*

[b]*College of Chemistry and Material Science, Huaibei Normal University, Huaibei, 235000, China*

[c]*College of Chemistry & Chemical Engineering, Anhui University, Hefei, 230601, China*

†Electronic supplementary information (ESI) available: Experimental section. See DOI: 10.1039/d0an02408b

Potential-resolved ratiometric ECL, in which the quantification depends on the ratio of two signals, could fulfil the requirement for multi-target analysis, and thus, it is an ideal approach to eliminate the interference factors and make the detection more convincing.[12] However, the strategies suffer from numerous challenges. For example, ECL emitters on one electrode may result in a cross-talk between the two ECL emitting processes, such as electrochemiluminescence resonance energy transfer (ECL-RET) between two ECL emitters.[13,14] This problem can be eased up by physically separating the working interface for different emitters.[15,16] However, the lack of well-matched potential-resolved ECL emitters that share the same coreactant limits the application fields of this technique. Sometimes the mixed coreactants are considered to realize two ECL signals for two ECL emitters within a given range of potential; however, it is still an imperfect way since some unclear side reactions may exist between the mixed coreactants or between ECL emitters and diversified coreactants. Besides, some ECL emitters usually have a similar excitation potential in the same coreactant. For example, both $Ru(bpy)_3^{2+}$ and g-C_3N_4 (or quantum dots, such as CdS QDs) can give ECL peaks in the range of −1.5 to −1.8 V in a $K_2S_2O_8$ solution, which results in the signal interference. Besides, $Ru(bpy)_3^{2+}$ and g-C_3N_4 have the possibility of undergoing ECL-RET.[17] However, in the tripropylamine (TPA) solution, only $Ru(bpy)_3^{2+}$ can be excited at a positive potential (about 1.3 V), thereby generating a strong ECL, while g-C_3N_4 fails. Though $Ru(bpy)_3^{2+}$ and g-C_3N_4 are two potential-resolved ECL emitters, the independent coreactants of TPA and $K_2S_2O_8$ are still in need since the cathodic ECL responses of $Ru(bpy)_3^{2+}$ and g-C_3N_4 interfere with each other in $K_2S_2O_8$. Therefore, to solve the above mentioned problems, the exploration of an easily-controlled and co reactant-separated ECL strategy is very appealing towards the ratiometric ECL analysis.

Conductive hydrogels have shown their potential as biosensors in the past years because they can be easily synthesized and could combine the soft materials with good conductivity.[18,19] Besides, they can retain water molecules and

maintain sufficient permeability, which makes them excellent electrode materials to achieve cell detection without the steric hindrance of cells.[20] With the excellent porous 3D nanostructure, polyaniline hydrogel (PAniH) can load numerous ECL molecules and maintain a stable ECL signal, which is weakly dependent on the number of cells,[21] and thus can act as a reference signal when we design a ratiometric ECL cytosensor.

In this study, a three-channel ratiometric ECL method for the MCF-7 cell analysis was proposed using three potential-resolved ECL probes, including g-C_3N_4, luminol-functioned gold nanoparticles (Lu–Au NPs), and $Ru(bpy)_3^{2+}$ doped silica nanoparticles ($RuSiO_2$ NPs). Proteoglycan CD44 and epidermal growth factor receptor (EGFR) are two over-expressed markers on the surface of MCF-7 cells.[22,23] MCF-7 cells were labeled with hyaluronic acid functionalized $RuSiO_2$ NPs (HA-RuSi) and epidermal growth factor functionalized g-C_3N_4 (EGF-g-C_3N_4) by the specific recognition of HA with CD44 and EGF with EGFR, respectively. As shown in Scheme 1, PAniH was modified on three working electrodes, namely GCE_A (WE 1), GCE_B (WE 2), and GCE_C (WE 3), as a detection platform for cells. For GCE_B, Lu–Au NPs were loaded on PAniH that provides a stable reference signal, which is rarely influenced by the number of cells on PAniH. The introduction of a reference ECL signal is necessary for a ratiometric assay because it can reduce the false positive or negative errors occurring during the detection of trace-level analytes in comparison with the single signal analysis. For GCE_A and GCE_C, g-C_3N_4 nanosheets and $RuSiO_2$ NP labeled cells provided two cell-dependent working signals, respectively. The as-prepared GCE_A, GCE_B, and GCE_C were placed in channels A, B, and C, respectively. Since the channels were spatially separated, coreactants $K_2S_2O_8$ and TPA could take part in the ECL reaction of g-C_3N_4 and $Ru(bpy)_3^{2+}$ in channel A and C, respectively, with luminol generating the ECL emission *via* dissolved oxygen in channel B. The simultaneous achievement of ECL_A, ECL_B, and ECL_C in a CV scan reflects the throughput analysis of multichannel ECL. Thus, during a CV scan, we can obtain three signals in the spatially-separated ECL system without interplay. The process of the fabrication of the cytosensor is given in detail in the ESI.† The concentrations of cells immobilized on the GCE_A and GCE_C can be quantified by the ratios of ECL_A/ECL_B and ECL_C/ECL_B, respectively.

Fig. 1A–C display the TEM images of g-C_3N_4 nanosheets, Ru SiO_2 NPs, and Lu–Au NPs, respectively. The size of most of the g-C_3N_4 nanosheets was less than 200 nm, and the Ru SiO_2 NPs are observed as spheres of around 70 nm diameter. Also, the size of Lu–Au NPs was around 20 nm. Besides, all the ECL probes had good dispersion. Further, the ultraviolet-visible (UV-Vis) absorption spectra of g-C_3N_4 nanosheets, RuSi NPs, and Lu–Au NPs are shown in Fig. S1.† The figure clearly shows that g-C_3N_4 nanosheets exhibit an absorption peak at 300 nm (Fig. S1A, ESI†). Peaks at 287 and 453 nm in the $RuSiO_2$ NP spectrum correspond to the π–π* electronic transition of bipyridine and metal-to-ligand charge transfer absorption, respectively, (Fig. S1B, ESI†). Similarly, Lu–Au NPs exhibits a broad absorption band at 250–400 nm corresponding to luminol and an absorption peak at 520 nm attributed to AuNPs (Fig. S1C, ESI†). These results are consistent with the previous literature.[7,16,24] Furthermore, the SEM images of PAniH exhibit a porous 3D coral-like microstructure (Fig. 1D), which is densely coated with numerous Lu–Au nanoparticles (Fig. 1E).

The ECL responses of the three-channel ratiometric ECL cytosensor were researched, and the results are shown in Fig. 2. The PAniH modified electrodes, GCE_A (WE 1), GCE_B (WE 2), and GCE_C (WE 3), gave almost no ECL signals (curve a). When Lu–Au NPs were immobilized on GCE_B/PAniH, a strong ECL emission peak corresponding to luminol (curve b) was observed. When HA-RuSi labeled cells, EGF-g-C_3N_4 labeled cells, and the two ECL probes labeled cells were immobilized on the GCE_C/PAniH, GCE_A/PAniH, and GCE_B/PAniH/Au, respectively, through the specific binding of FA on the electrode with FA receptors on the cell surface, WE 1 and WE 3 displayed two significant ECL responses, while the ECL intensity of WE 2 was nearly not affected by the cells (curve c). This stable ECL response of WE 2 can be ascribed to the porous structure of PAniH that keeps numerous water molecules and allows the fast exchange of dissolved oxygen below the cells, thereby supporting the stable ECL reaction of luminol.

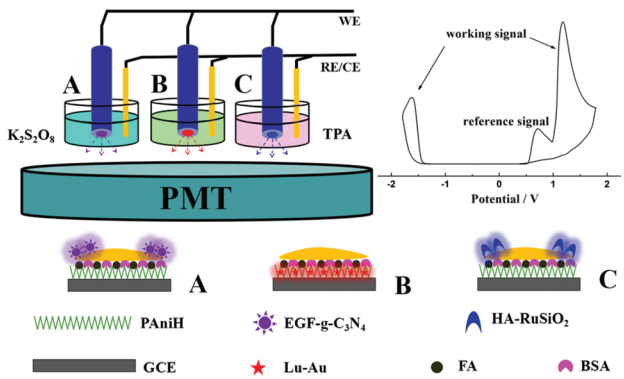

Scheme 1 The schematic illustration of the three-channel ratiometric ECL platform for MCF-7 cell quantification.

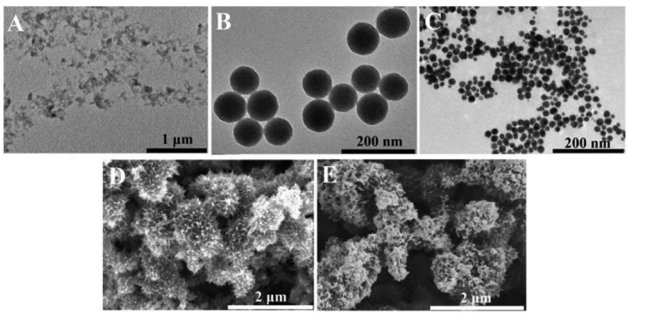

Fig. 1 TEM images of g-C_3N_4 nanosheets (A), $RuSiO_2$ NPs (B) and Lu–Au NPs (C). SEM images of PAniH (D) and Lu–Au NPs on PAniH (E).

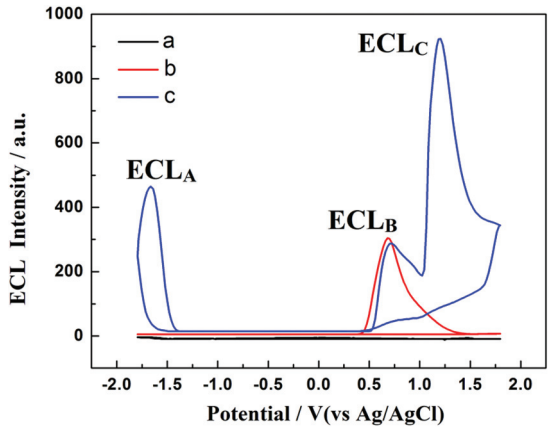

Fig. 2 Potential-resolved ECL curves of PAniH (a), PAniH with Lu–Au NPs (b), and PAniH with Lu–Au NP and ECL probes labeled cells (c). ECL_A, ECL_B, and ECL_C were obtained in the solution containing 0.1 M $K_2S_2O_8$, 0.01 M PBS, and 0.1 M TPA, respectively.

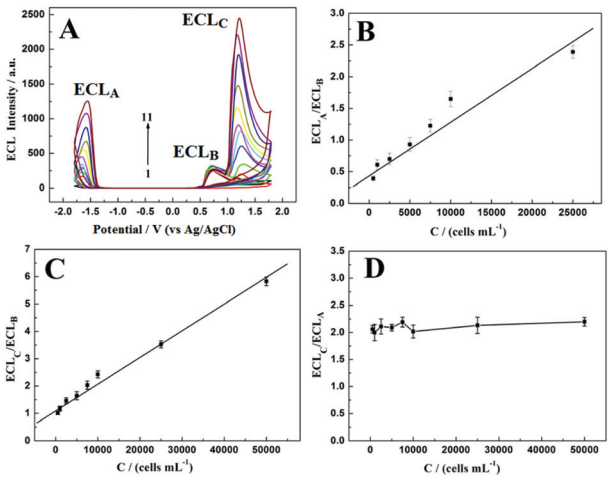

Fig. 3 Potential-dependent ECL curves when the concentration of MCF-7 changes from 5.0×10^2 (curve 1) to 2.5×10^5 cells per mL (curve 11) (A). Correlation of the ECL_A-to-ECL_B ratio and the cell concentration (B). Correlation of the ECL_C-to-ECL_B ratio and the cell concentration (C). Correlation of the ECL_C-to-ECL_A ratio and the cell concentration (D). ECL_A, ECL_B, and ECL_C were obtained in the solution containing 0.1 M $K_2S_2O_8$, 0.01 M PBS, and 0.1 M TPA, respectively.

Furthermore, the positive role of luminol as a reference signal can be applied in correcting the changes of the photomultiplier tube voltage (PMT), as shown in Fig. S2A (ESI†). From the result, we can see that the ECL intensities of g-C_3N_4, luminol, and $Ru(bpy)_3^{2+}$ increased when the PMT voltage was increased from 300 to 800 V. However, the ratio of ECL_A/ECL_B and ECL_C/ECL_B are almost the same, as shown in Fig. S2B (ESI†). The result thus demonstrates that external factors such as PMT voltage could influence the detecting result if only one luminophore (g-C_3N_4 or $Ru(bpy)_3^{2+}$) is used in the system. However, when another luminophore (luminol) is used as a reference signal, the cytosensor for cancer cell quantification will be improved with high accuracy.

The optimization of experimental conditions was also carried out and is shown in Fig. S3 (ESI†). Upon fixing the experimental conditions, the as-prepared ECL cytosensor was employed to detect the number of MCF-7 cells, with the help of $Ru(bpy)_3^{2+}$ and g-C_3N_4 nanoprobes tagged on the surface of the cells. The ECL signal of $Ru(bpy)_3^{2+}$ and g-C_3N_4 varied with the number of cells, while the luminol signal remained stable, as demonstrated in Fig. 3A. Herein, the ECL of $Ru(bpy)_3^{2+}$ and g-C_3N_4 served as the analytical signals, and the ECL of luminol acted as the reference signal. Further, the ratio of ECL_A/ECL_B and ECL_C/ECL_B presented two linear relationships with the cell concentration (Fig. 3B and C), and the corresponding linear ranges, detection limits, *etc.*, are listed in Table S1 (ESI†). Therefore, two different approaches to detect MCF-7 cells were simultaneously obtained, and their testing results were basically consistent with each other, which increased the credibility of MCF-7 cells diagnosis. In addition, the ECL ratio of $Ru(bpy)_3^{2+}$ to g-C_3N_4 (ECL_C/ECL_A, about 2.1) showed negligible variation with the cell concentration (Fig. 3D), suggesting the stable expression of CD44 and EGFR on each cell. Furthermore, the ratio of ECL_C/ECL_A can be used to distinguish MCF-7 cells from other cells because of the different degrees of expression of CD44 and EGFR in different types of cells. For example, we detected the human skeletal muscle cells (HSMC, normal cells, whose cell surface shows low-expression of CD44 and EGFR, particularly EGFR) with the proposed method, and the ratio of ECL_C/ECL_A (about 3.5) was higher than that of MCF-7 cells.[25,26]

Different cell lines, such as RAW 264.7 (murine macrophages), H9C2 (cardiac myocytes), and HSMC (human skeletal muscle cells), were chosen as models to evaluate the cytosensor selectivity, and the ECL intensity is shown in Fig. S4.† Small ECL signal changes were observed, except for MCF-7, indicating that the ECL strategy has excellent selectivity towards MCF-7 cells. The reproducibility of the cytosensor was evaluated by assaying a 1.0×10^4 cells per mL cell solution. Experimental results indicated that the RSD (n = 5) of the intra-assay were 4.1% and 5.3% for ECL_A and ECL_C, respectively, whereas the RSD of the inter-assay with various batches were 5.5% and 5.7% (n = 5) for ECL_A and ECL_C, respectively. Hence, both intra-assay and inter-assay revealed a good reproducibility of the cytosensor.

In summary, a ratiometric ECL cytosensor based on PAniH was constructed in spatially separated ECL systems using three potential-resolved ECL probes, namely g-C_3N_4, Lu–Au NPs, and $RuSiO_2$ NPs. Lu–Au NPs on PAniH presented a stable ECL response that is weakly dependent on the number of cells, thus serving as the reference standard signal. Moreover, g-C_3N_4 and $RuSiO_2$ NPs were tagged on the surface of MCF-7 cells and used as detection signals. On account of the overexpressed EGFR and CD44 on the cell surface, the ECL cytosensor simultaneously supported two reliable methods of detecting MCF-7 cells. Therefore, this study exhibits the feasibility of the multichannel ECL detection and demonstrates great potential in the multi-biomarker analysis and the early

diagnosis of cancers. Thus, apart from improving the throughput, future efforts should be directed towards synthesizing potential-resolved or spectrum-resolved ECL probes, designing multi-channel ECL cells, assembling electrochemical arrays, fabricating integrated circuit microplates, and developing ECL imaging devices.

Conflicts of interest

The authors declare that they have no conflict of interest.

Acknowledgements

This work was supported by the National Natural Science Foundation of China (Grants No. 21427807), Anhui Provincial Natural Science Foundation (Grants No. 2008085QB68) and Foundation of State Key Laboratory of Analytical Chemistry for Life Science (Grants No. SKLACLS2003).

Notes and references

1 Y. N. Khonsari and S. Sun, *Chem. Commun.*, 2017, **53**, 9042–9054.
2 W. Gao, Y. Liu, H. Zhang and Z. Wang, *ACS Sens.*, 2020, **5**, 1216–1222.
3 J. Zhang, R. Jin, D. Jiang and H. Y. Chen, *J. Am. Chem. Soc.*, 2019, **141**, 10294–10299.
4 W. Guo, H. Ding, C. Gu, Y. Liu, X. Jiang, B. Su and Y. Shao, *J. Am. Chem. Soc.*, 2018, **140**, 15904–15915.
5 H. Zhang, B. Li, Z. Sun, H. Zhou and S. Zhang, *Chem. Sci.*, 2017, **8**, 8025–8029.
6 H. Ding, W. Guo and B. Su, *Angew. Chem.*, 2020, **132**, 457–464.
7 H. Gao, W. Han, H. Qi, Q. Gao and C. Zhang, *Anal. Chem.*, 2020, **92**, 8278–8284.
8 D. Long, Y. Shang, Y. Qiu, B. Zhou and P. Yang, *Biosens. Bioelectron.*, 2018, **102**, 553–559.
9 H. Dai, G. Xu, S. Zhang, Z. Hong and Y. Lin, *Chem. Commun.*, 2015, **51**, 7697–7700.
10 L. Ding, S. Xu, D. Huang, L. Chen, P. Kannan, L. Guo and Z. Lin, *Analyst*, 2020, **145**, 6524–6531.
11 X. Fu, X. Tan, R. Yuan and S. Chen, *Biosens. Bioelectron.*, 2017, **90**, 61–68.
12 H. R. Zhang, J. J. Xu and H. Y. Chen, *Anal. Chem.*, 2013, **85**, 5321–5325.
13 F. R. Liu, J. T. Cao, Y. L. Wang, X. L. Fu, S. W. Ren and Y. M. Liu, *Sens. Actuators, B*, 2018, **276**, 173–179.
14 J. T. Cao, F. R. Liu, X. L. Fu, J. X. Ma, S. W. Ren and Y. M. Liu, *Chem. Commun.*, 2019, **55**, 2829–2832.
15 X. Feng, N. Gan, S. Lin, T. Li, Y. Cao, F. Hu, Q. Jiang and Y. Chen, *Sens. Actuators, B*, 2016, **226**, 305–311.
16 X. Feng, N. Gan, H. Zhang, Q. Yan, T. Li, Y. Cao, F. Hu, H. Yu and Q. Jiang, *Biosens. Bioelectron.*, 2015, **74**, 587–593.
17 Q. M. Feng, Y. Z. Shen, M. X. Li, Z. L. Zhang, W. Zhao, J. J. Xu and H. Y. Chen, *Anal. Chem.*, 2016, **88**, 937–944.
18 N. Hao, R. Hua, S. Chen, Y. Zhang, Z. Zhou, J. Qian, Q. Liu and K. Wang, *Biosens. Bioelectron.*, 2018, **101**, 14–20.
19 D. Zhai, B. Liu, Y. Shi, L. Pan, Y. Wang, W. Li, R. Zhang and G. Yu, *ACS Nano*, 2013, **7**, 3540–3546.
20 G. Liu, C. Ma, B. K. Jin, Z. Chen, F. L. Cheng and J. J. Zhu, *Anal. Chem.*, 2019, **91**, 3021–3026.
21 C. Ding, Y. Li, L. Wang and X. Luo, *Anal. Chem.*, 2019, **91**, 983–989.
22 Y. Qiu, B. Zhou, X. Yang, D. Long, Y. Hao and P. Yang, *ACS Appl. Mater. Interfaces*, 2017, **9**, 16848–16856.
23 B. Zhou, Y. Qiu, Q. Wen, M. Zhu and P. Yang, *ACS Appl. Mater. Interfaces*, 2017, **9**, 2074–2082.
24 L. S. Lin, Z. X. Cong, J. Li, K. M. Ke, S. S. Guo, H. H. Yang and G. N. Chen, *J. Mater. Chem. B*, 2014, **2**, 1031–1037.
25 E. Mylona, K. A. Jones, S. T. Mills and G. K. Pavlath, *J. Cell. Physiol.*, 2006, **209**, 314–321.
26 A. Uezum, M. Nakatani, M. Ikemoto-Uezumi, N. Yamamoto, M. Morita, A. Yamaguchi, H. Yamada, T. Kasai, S. Masuda, A. Narita, Y. Miyagoe-Suzuki, S. Takeda, S. Fukada, I. Nishino and K. Tsuchida, *Stem Cell Rep.*, 2016, **7**, 263–278.

